LAJSBA
LATIN AMERICAN JOURNAL OF SEDIMENTOLOGY AND BASIN ANALYSIS | VOLUME 32 (2) 2025, 103-120

MISMOS (MICROSCALE MORPHOLOGY SYSTEM): AN INEXPENSIVE NEW METHOD TO SURVEY 3D SURFACE MICROMORPHOLOGY

Yajaira C. Alquinga Salazar[1], Sibila A. Genchi[1,2], Lucas Nuciari[2], Vanesa L. Perillo[2,3], M. Cintia Piccolo[1,2], Gerardo M. E. Perillo[2,4]*

[1] Departamento de Geografía y Turismo, Universidad Nacional del Sur, 12 de octubre 1098, Bahía Blanca, Argentina, B8000CTX
[2] Instituto Argentino de Oceanografía (IADO, CONICET/UNS), Camino La Carrindanga Km 7 E1, Bahía Blanca, Argentina, B8000CPB
[3] Departamento de Biología, Bioquímica y Farmacia, Universidad Nacional del Sur, Bahía Blanca, Argentina, B8000ICN
[4] Departamento de Geología, Universidad Nacional del Sur, Alem 1253, Bahía Blanca, Argentina, B8000ICN
*Corresponding author: cristinalquinga@gmail.com

ARTICLE INFO

Article history
Received July 12, 2024
Accepted March 12, 2025
Available online April 16, 2025

Handling Editor
José I. Cuitiño

Keywords
Portable survey system
MiSMoS testing
Micromorphology mapping
Beach

ABSTRACT

Microscale morphology in coastal environments is complex to study due to both the large spatial and temporal variability. No direct instrumentation is available to map the micromorphology in detail. The aim of this article is to describe the application of the newly developed MiSMoS (MicroScale Morphology System) methodology for mapping surface and small-scale morphologic features such as ripples, rills, and small courses, as well as to demonstrate its advantages and limitations. A set of measurements on a perched beach that offers varied microforms was carried out as a case study example. The MiSMoS consists of a table of 1.6 m x 1.6 m square aluminum structure with six L-shaped rails on top to mobilize a sensor-carrying structure, which is supported on 4 legs (0.60 m high). The sensor-carrying structure is built with two cameras and a Laser Distance Meter (LDM), with cameras at a fixed angle of 20°. In the operating procedure for high-resolution mapping, the sensor-carrying structure is manually moved sequentially capturing images that cover a surface of 0.60 x 0.60 m, with 75% overlap. High-resolution 3D models were generated from the images using Structure-from-Motion, Multi-View-Stereo (SfM-MVS) technique. MiSMoS has numerous advantages over commercial instrumentation: 1) it can map topography at a high resolution, 2) it is easy to build and deploy, 3) it is inexpensive, and 4) in one operation, a high-resolution map of an area of 2.25 m^2 can be obtained in about 15-20 min, whereas other systems usually only provide profiles.

INTRODUCTION

Landform micromorphology plays a pivotal role in various ecological, hydrological, and biogeochemical processes. However, quantifying micromorphological characteristics presents a significant challenge in data acquisition. Research on micro-scale landforms often primarily focuses on laboratory experiments, while field surveys are frequently neglected (Bupo and Weber, 2017). Current microtopography studies

achieve spatial resolutions smaller than one meter, primarily focusing on detecting surface heterogeneity (Shukla *et al.*, 2023). Despite these advancements, standardized and systematic methodologies incorporating small format instruments for micromorphology surveys, as well as the development of micromorphological models applicable to natural ecosystems, are still lacking.

Photogrammetric techniques are valuable for mapping and studying morphology/topography in various environments. Conventional aerial and satellite sensors can cover extensive areas with resolutions ranging from centimeters to hundreds of meters (Nesbit and Hugenholtz, 2019; Nakata *et al.*, 2023). A technique for three-dimensional morphological analysis thought image overlay evolved significantly with the advent of Structure-from-Motion, Multi-View-Stereo (SfM-MVS) (Remondino and Fraser, 2006). SfM-MVS represents an automated, high-resolution, and cost-effective method for acquiring spatial and optical information (Genchi *et al.*, 2015). While it is extensively utilized for characterizing morphological changes particularly in coastal areas, studies employing SfM-MVS often overlook the recording of micromorphology.

Various methods exist for measuring beach forms, ranging from simple to precise and sophisticated techniques. The feasibility of measuring morphology at small scales may be constrained by beach accessibility and the costs of acquiring equipment. For example, Otvos (1999) proposed the use of rules with yard and inch-graduations to study relief forms generated by groundwater seepage and surface runoff. The limitation of adjusting the rules according to the size of the landform prolongs the survey time, and their placement on the studied structure may disturb it.

Another important mechanical instrument for profiling geoforms in coastal environments, such as bedforms on a beach, was developed by Sherman *et al.* (1993). They describe a micromachined surface sensor made of aluminum called "comb", measuring 1 meter in length, with teeth 0.40 meters long and spaced at 0.10 m apart. The operation of the comb involved pushing the device into the sand, perpendicular to the orientation of the bedform, and the length of the teeth allowed for determining the height and length, which were then recorded manually. To map the surface, the authors proposed to set up a series of parallel lines; however, data recording was restricted to a coarse spacing, resulting in the loss of many details.

In addition, an ultrasonic sensor system was designed to assess natural beaches for the X-SHORE project. It was employed to observe and quantify changes in the seabed level wave by wave in the swash zone (Turner *et al.*, 2008). The 2D structure has a height of 0.8 m above the surface; the sensor records data at a frequency of 4 Hz with an accuracy of approximately ± 0.01 m. Despite these advantages, the limitation is given by the high cost of acquiring.

The commercially available Sand Ripple Profiler must be positioned on a support at an adequate height above the surface. The system scans 2 m long lines of the surface every minute (Miles *et al.*, 2014). The advantage of the Sand Ripple Profiler is that it scans the beach surface when ripples are actively influenced by waves and currents, and the results show their temporal evolution with high resolution. However, it only provides a cross-sectional profile of the beach.

The study by Agüera-Vega *et al.* (2020) on micromorphology considers crucial parameters in the accuracy of Digital Elevation Models (DEM); such as point cloud density and grid size. Current studies on micromorphology typically achieve spatial resolutions of less than 1 m and emphasize the implementation of technologies for detecting surface heterogeneity yet lack standardized methodologies for incorporating sensors and developing micromorphological models in natural ecosystems (Nouwakpo *et al.*, 2016; Ehrhardt *et al.*, 2022; Li *et al.*, 2022).

Based on the of the above-mentioned state-of-the-art for landform micromorphology survey, the aim of this article is to describe the application of the newly developed MiSMoS (MicroScale Morphology System) methodology for mapping surface and small-scale morphologic features such as ripples, rills and small courses, as well as to demonstrate its advantages and limitations. A set of measurements on a perched beach that offers varied microforms was carried out as a case study example.

METHODOLOGY

The methodology for this study was structured into three main parts: preprocessing, processing, and post-processing. Micromorphology mapping was conducted on the beach of Pehuén Co city, Buenos Aires Province, Argentina (39°00'16" S, 61°32'53.50" W). This selection was based on the availability of scheduled campaigns for Pehuén Co. This study focused on a coastal environment; however, the methodology is broadly applicable to diverse environmental systems. A workflow diagram is presented to guide the process (Fig. 1).

Description of MiSMoS

MiSMoS (Perillo *et al.*, 2022) (Fig. 2) was developed for micromorphology mapping. It consists of a table composed of a 1.60 m x 1.60 m square aluminum structure with six L-shaped aluminum rails on top to mobilize a sensor-carrying structure (*i.e.*, two cameras and a Laser Distance Meter (LDM)), which is supported on 4 legs (0.60 m high). The rails, supports, curtains, among other pieces (totaling approximately 38 kg) are stored and transported in a specially designed bag (Fig. 2a).

An inspection of all pieces prior to the start of assembly is recommended. The assembly process involves placing the four supports and the four brackets on the chosen site (Fig. 2b-d). Then, the six rails are positioned at the top of the table, arranged parallel to one side with a separation of 0.32 m (Fig. 2e); this separation ensures maximum image overlap. The rails serve two purposes: 1) to move the sensor-carrying structure along the top of the rails and, 2) to support panels (Fig. 2f) to prevent light penetration.

The undesired effect of external light was controlled using rectangular vinyl panels (1.6 m long, 0.32 m wide, and 0.003 m thick). Furthermore, the sides were covered with black faux leather fabrics, 1.6 m long and 0.5 m wide (Fig. 3a), supported by iron bars inserted at the top or/and bottom ends. The black faux leather fabric was initially fixed to the legs with adhesive tape (Fig. 3a), but in a more advanced version, VELCRO strips were used, allowing for better adaptation and closure (Fig. 3b).

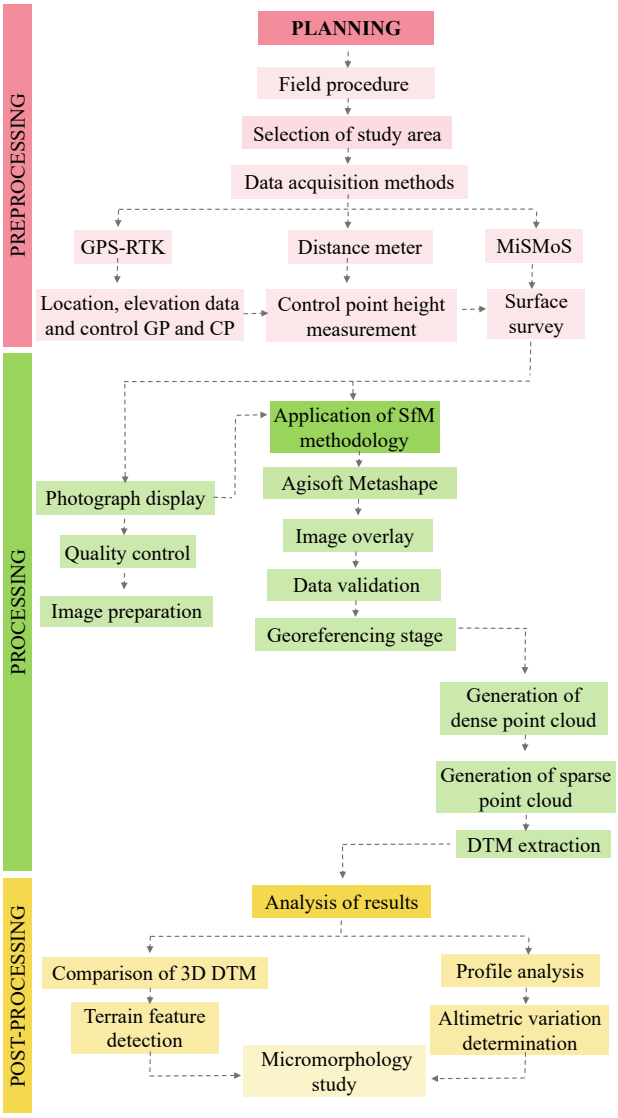

Figure 1. Workflow diagram used for the study of micromorphology using MiSMoS.

The sensor-carrying structure was designed using Sketchup software and fabricated using the 3D printer available at the Instituto Argentino de Oceanografía (IADO). The dimensions of the structure are 0.28 m long, 0.29 m wide, and 0.003 m thick (Fig. 4c). The sensor-carrying structure was designed to be moved manually over the rails. The two-camera system consists of mobile phones Xiaomi 5G (Fig. 4a), with a focal length of 4.695 mm and ISO 3208. The cameras are positioned at 0.6 m above the surface to be surveyed, covering a surface of 0.6 x 0.6 m, with 75% overlap.

The two-camera system is used when composing images into the resulting stereoscopic format; it is required that the two images of

Figure 2. MiSMoS assembly stages. **a)** Storage of MiSMoS pieces, **b)** pre-assembly inspection of the structure, **c)** addition of supports and screws, and **d)** placement of supports for curtains. **e)** Incorporation and adjustment of aluminum rails to the MiSMoS structure frame, and **f)** movement of the sensor-carrying and panels that block light during the survey.

Figure 3. External light control. **a)** side section covered curtains and the black faux leather fabrics secured to the structure supports with tape, and **b)** supports velcro straps on the sides.

the stereo pair, from both the left and the right cameras, be line-aligned (Hasmanda and Riha, 2012), leading to the perception of depth in the scene. The cameras were positioned at an angle of 20° on each side (Fig. 4b), obtaining an oblique image angle recommended for nadir image blocks (Nesbit and Hugenholtz, 2019). This arrangement created a fixed triangular support. The specific angle is a fixed parameter and allows for a better stereoscopic scene perception.

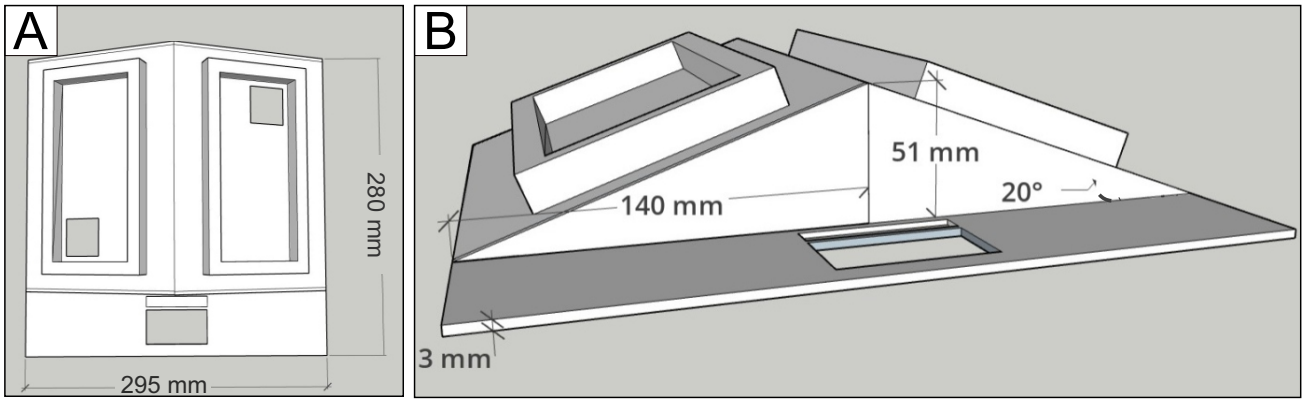

Figure 4. Sketch of the sensor-carrying structure dimensions. **a)** Plane view and **b)** profile view.

A support for the LDM (0.057 m long, 0.05 m high, and 0.1 m wide) is incorporated into the sensor-carrying structure. The opening (0.32 m wide and 0.57 m long) is located at the front of the structure (Fig. 4) and allows the laser to point vertically at the surface to be surveyed. The LDM used is a BOSCH DLE 50 PROFESSIONAL and has a measuring range from 0.05 to 50 m with a measurement precision of ± 0.0015 m (BOSCH, 2017). The LDM measures in each ground control point (GCP).

A set of markers acting as GCP were designed in Sketchup software (Fig. 5a) and fabricated using the 3D printer. The dimensions of the surface disks are 0.02 m in diameter and 0.003 m in thickness (Fig. 5b), which were chosen to avoid interference with microforms and to ensure the cameras could capture them for easy identification in the obtained images (Fig. 5c,d).

Field Procedure

The MiSMoS is mobilized and placed by a team of two to four people, avoiding disturbances in the surface to be surveyed. In each sector, a total of eight markers were placed in a regular spaced pattern. Besides, the position of each marker is perpendicular to the beam of light of the LDM (defined position). The location of the GCP was established so they could be covered by at least two photos, ensuring better analysis for the SfM-MVS technique. The survey starts with sequentially taken measurements. We take measurements of each sector at a fixed point in time. The survey was conducted from the beginning of low tide and throughout most of the ebb tide, because we had the increased extent of exposed beach. The start and end time of the survey were recorded to estimate the survey interval, ranging from 15 to 20 min.

The sensor-carrying structure is moved along a rail, capturing photos every 0.28 m, *i.e.*, the length of the sensor-carrying structure (Fig. 6a). The consistent distance for each shot is ensured through marks placed on the supports. A total of 60 photos are taken, with 30 photos per mobile phone. Heights were measured using the LDM simultaneously with photo capture (Fig. 6b), and these data were recorded in a spreadsheet. This procedure was repeated for each rail to complete the sequence of five rails, named alphabetically from A to E.

Finally, once MiSMoS is removed, GCP remains (Fig. 7a). An Emlid Reach RS2 receiver was used as a base station using RTK-NTRIP technology, using corrections provided by the Instituto Geográfico

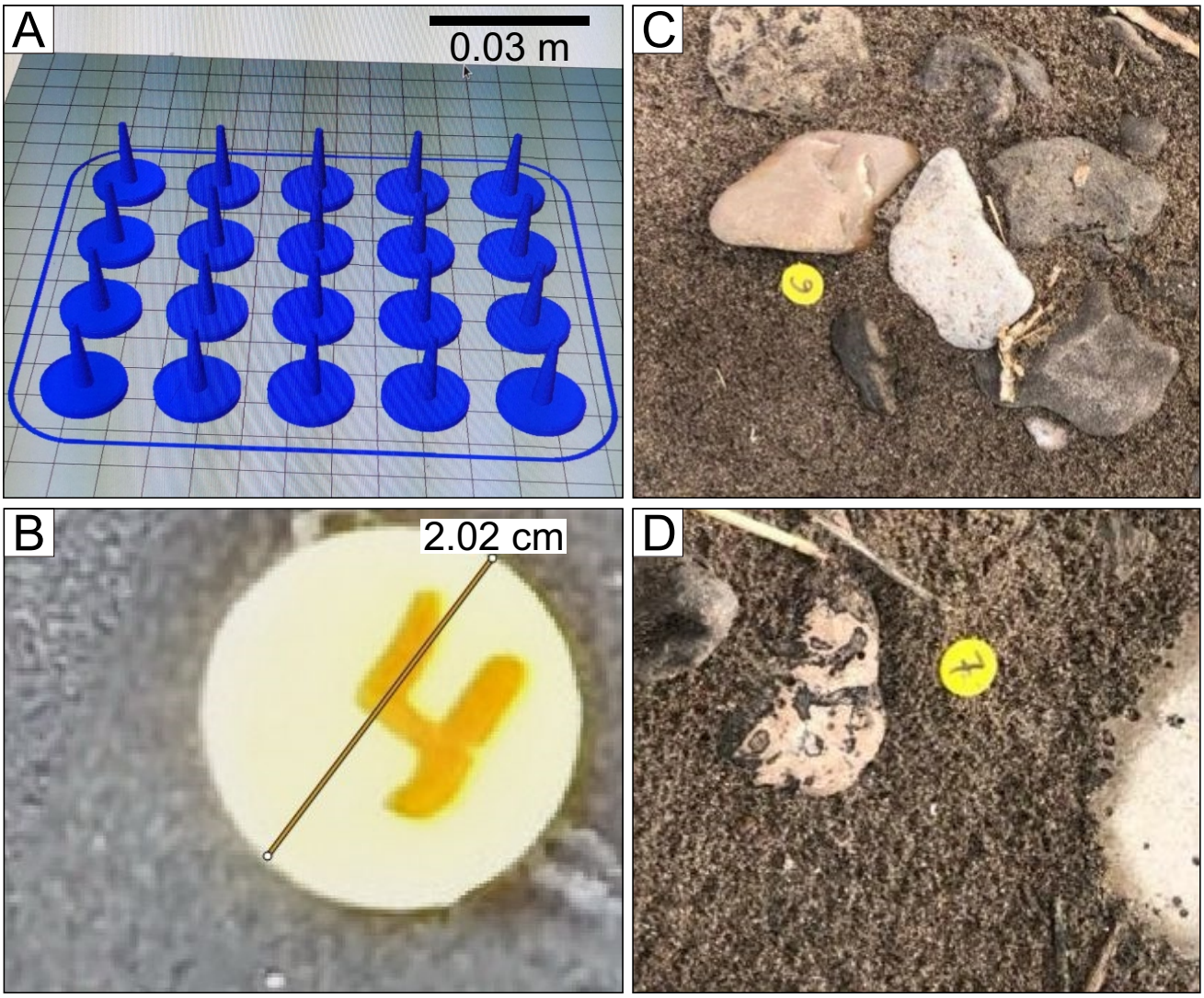

Figure 5. Ground control points. **a)** Designed in Sketchup, **b)** marker diameter measured on the model, **c)** and **d)** positioned in the survey sector.

Nacional, with their permanent reference station (BATE-v3.0) located approximately 40 km from the study area. After establishing the base station, another Emlid Reach RS2 receiver configured as a mobile rover recorded the GCP and CP which were corrected from the base station (Fig. 7b). The precision of positioning depends essentially upon the range between rover and base (Matias *et al.*, 2015); the error signal are constants on both GPS receivers (base and rover) and therefore the errors can be minimized. In this study, the range was less than 0.5 km; therefore, the horizontal error was 0.007 m and the vertical error was 0,014 m.

Imagen Acquisition Assessment

Two image capture approaches were compared in this study: the MiSMoS and conventional digital photogrammetry. The second method involved using a handheld camera to capture the surface from different angles without a fixed structure. Photographs were acquired to evaluate the effectiveness of each method for surface reconstruction. Photographic control was conducted to ensure image quality and consistency. Additionally, the assessing was to determine if any deformation occurred in the surface reconstruction.

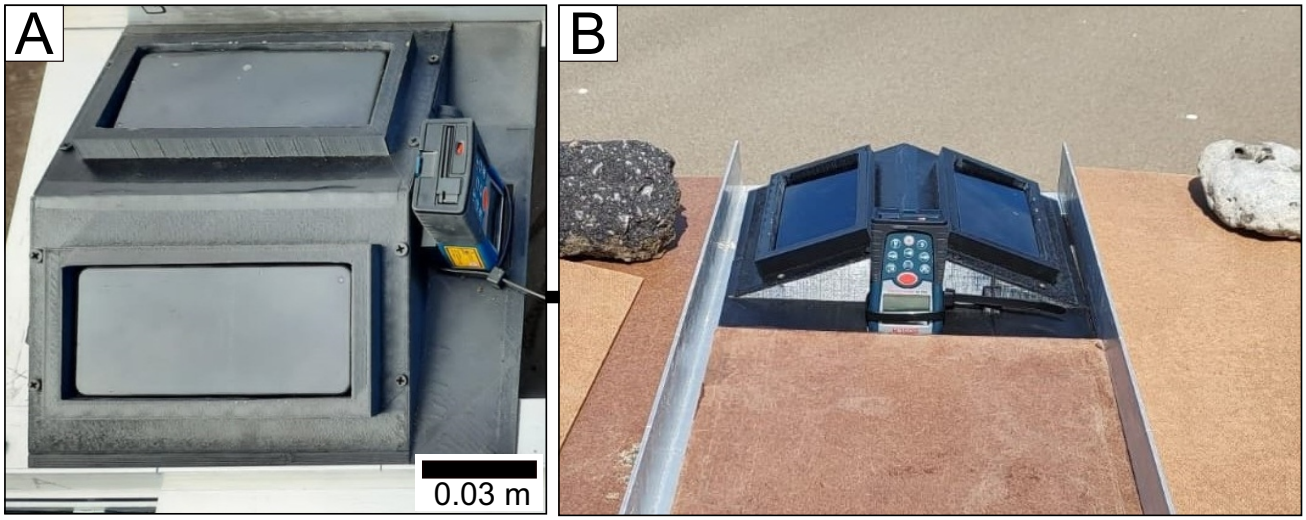

Figure 6. Micromorphology survey **a)** Start of photos and height measurements, red line separation mark, and **b)** sensor-carrying and vinyl panels during the survey.

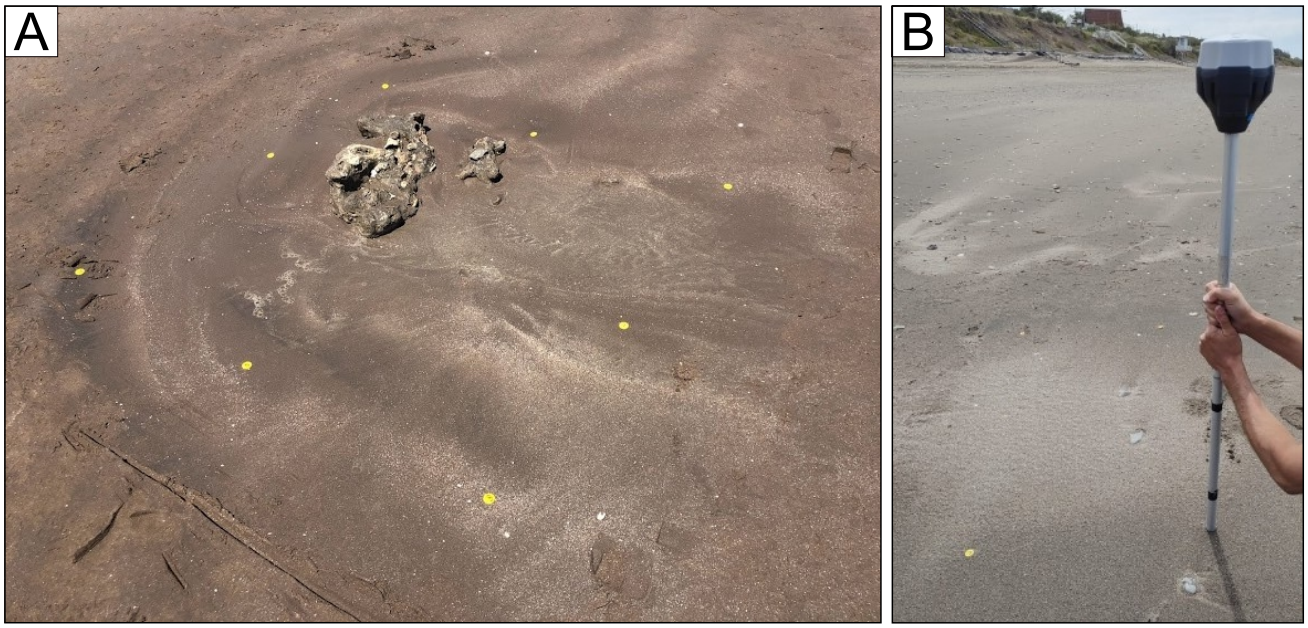

Figure 7. Coordinate acquisition with GPS. **a)** Ground control points after MiSMoS were removed. **b)** Receiver positioned over a marker collecting GPS data using RTK-NTRIP technology.

Postprocessing

The quality control of photos from each mapping sector begins by visualizing all digital images using Microsoft® Photos 2020 software. Duplicated photos are eliminated, and a selection is made for those needing editing. Adjustments to saturation, levels, and contrast are performed using Adobe Photoshop 2019 editing software.

In the second stage, SfM-MVS methodology is applied to the pre-checked images, which are then loaded into Agisoft Metashape® software. At first, low, medium, and high resolutions were tested to determine the best resolution and less processing time. As low and medium resolution did not provide the desired quality for point cloud, processing was conducted at high resolution to construct the dense point cloud for

each mapping. This choice aimed to accurately represent the most significant features in the DEMs.

The dense point cloud was processed in part in Agisoft Metashape®. In addition, a set of postprocessing was made using the open-source software CloudCompare. The dense point cloud was segmented into sections orthogonal to the x-axis. These sections were created at regular intervals with a predefined length of 1.6 m and a separation of 0.1 m. Each section was represented as an independent point cloud with vertical topography variability.

The scripts were generated in the open-source software R. The variations in DEM height were visualized in a 2D graph with a color scale. Cross-sectional profiles were generated from segments obtained from the dense point cloud in CloudCompare, selecting those with the greatest variability.

Finally, the heights measured with the LDM at each GCP on each sector are compared to the marker (GCP and CP) heights in the DEM, as visualized in the dense point cloud in CC. A script was developed to calculate the coefficient of determination through linear regression. The results are expected to align closely with the regression line, with the proximity or coincidence of the observed points to the line determined by the measurement error (Dagnino, 2014).

TESTING THE MiSMoS IN DIFFERENT CASE STUDIES

To evaluate the capability of the MiSMoS methodology for studying micromorphology, we analyzed the DEM of surfaces with varying complexity. The selected sectors ranged from relatively flat to more intricate terrains. Additionally, calibrated cross-sections were used to demonstrate methodological quality.

The study cases for micromorphology mapping are located at Pehuén Co City, Argentina (Fig. 8a). This beach is intermediate-dissipative, characterized by mixed fine sand, gravels, and significant rock outcrops (Perillo *et al.*, 2011; Bustos *et al.*, 2021) (Fig. 8). It is subject to significant surficial seepage of groundwater, which is a mixture of freshwater discharge from dunes and infiltration of sea water from the previous tide (Andes, 2018). Here, we present significant examples representing surfaces of different complexity (Table 1). We measured in three sectors for validation and testing of the MiSMoS capability to analyze microtopography.

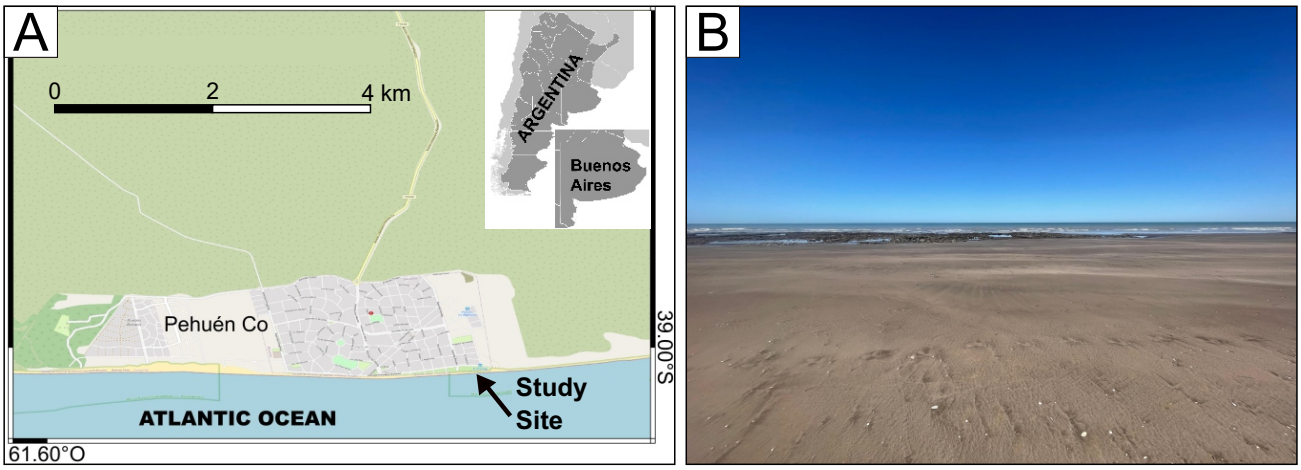

Figure 8. Location of the study area. **a)** Location of Pehuén Co Beach in Argentina, **b)** view from the place where the examples shown in the present article were taken.

Micromorphology description

The Sector 1 displays a relatively simple surface comprising sand with dispersed pebbles (Fig. 9a,b). Marine bioclasts (shell fragments) exhibit rounded shapes, with diameters ranging from 0.020 to 0.044 m (Fig. 9c). Angular clasts of different sizes, ranging from 0.023 to 0.052 m, are oriented in various directions (Fig. 9d), with discernible adjacent erosion marks.

Test Sector	Main morphology features	Measures	
		GPS	LDM
1	Surface of sand with dispersed pebble clasts on the front shore	x	x
2	Surface of sand with dispersed pebbles on the backshore	x	x
3	Complex, sandy and rocky surface with differential erosion in the swash-zone	x	x

Table 1. Examples representing surfaces of different complexity and measurement using GPS and LDM.

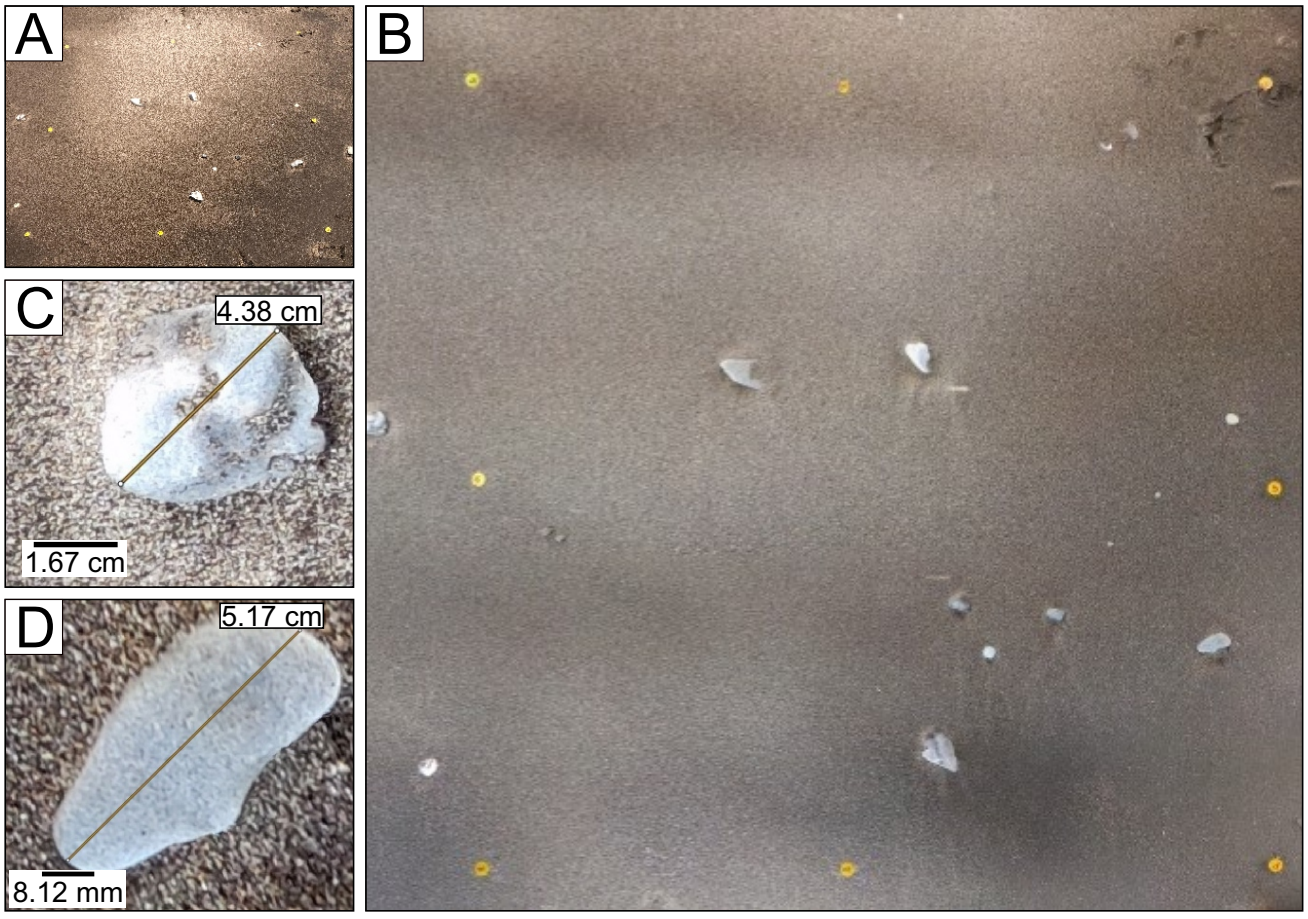

Figure 9. Results from Test sector 1. **a)** A photograph of a simple sandy surface with dispersed pebbles on the foreshore. **b)** Preliminary orthomosaic extracted using the SfM-MVS technique. Measurements of pebble size of **c)** and **d)** were taken on the dense point cloud. Yellow circles represent the GCP and CP markers.

The DEM from Test Sector 1 (Fig. 10) illustrates height variations across the relatively flat surface, ranging from 0.00 to 0.04 m. Maximum elevations of 0.03 and 0.04 m correspond to pebbles depicted in yellow and red on the height scale of the DEM. Minimal elevations of 0.01 and 0.02 m are distributed on the surface. These height variations are evident in microprofiles (Fig. 10b-e) derived from selected sectors in the DEM. The peaks (Fig. 10) correspond to pebble clasts distributed heterogeneously on the simple geomorphology. Depressions 0.002 m deep are observed around clasts embedded in the sand. The lowest height of 0.034 m is at microprofile P1 on a bioclast (Fig. 10b), while the highest heights of 0.036 and 0.042 m are found on angular pebble clasts (Fig. 10c, d, and e).

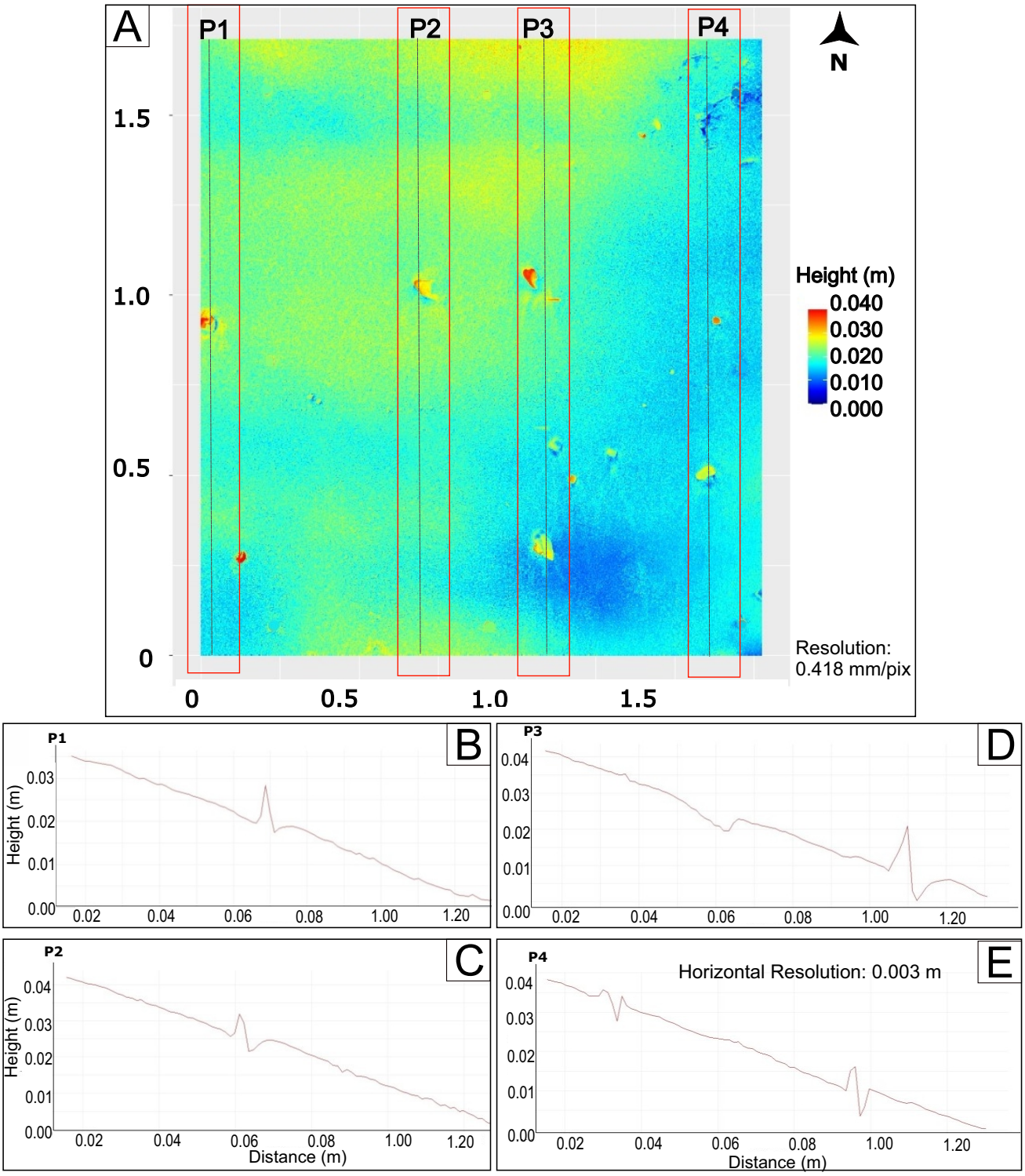

Figure 10. Results from a survey using MiSMoS at Test Sector 1. **a)** Digital Elevation Model with the position of the microprofiles P1, P2, P3 and P4 are indicated. **b)** Microprofile 1, featuring a bioclast in sand, **c)**, **d)** and **e)** taken over angular clasts without preferred orientation.

For surfaces of medium complexity (Fig. 11a), a variety of pebble clasts of different sizes and origins are observed (Fig. 11b). Clasts range from angular to rounded, with lengths between 0.108 and 0.112 m (Fig. 11 c-e). This surface also features vegetable elements (Fig. 11c). In the DEM (Fig. 12 a), a maximum height of 0.16 m is depicted in red, while minimum values range from 0.00 to 0.04 m, in blue and light blue. Microprofiles (Fig. 12b-e) display minimal variation compared to previous profiles, attributed to clast and vegetal branch fragments distributed across the surface.

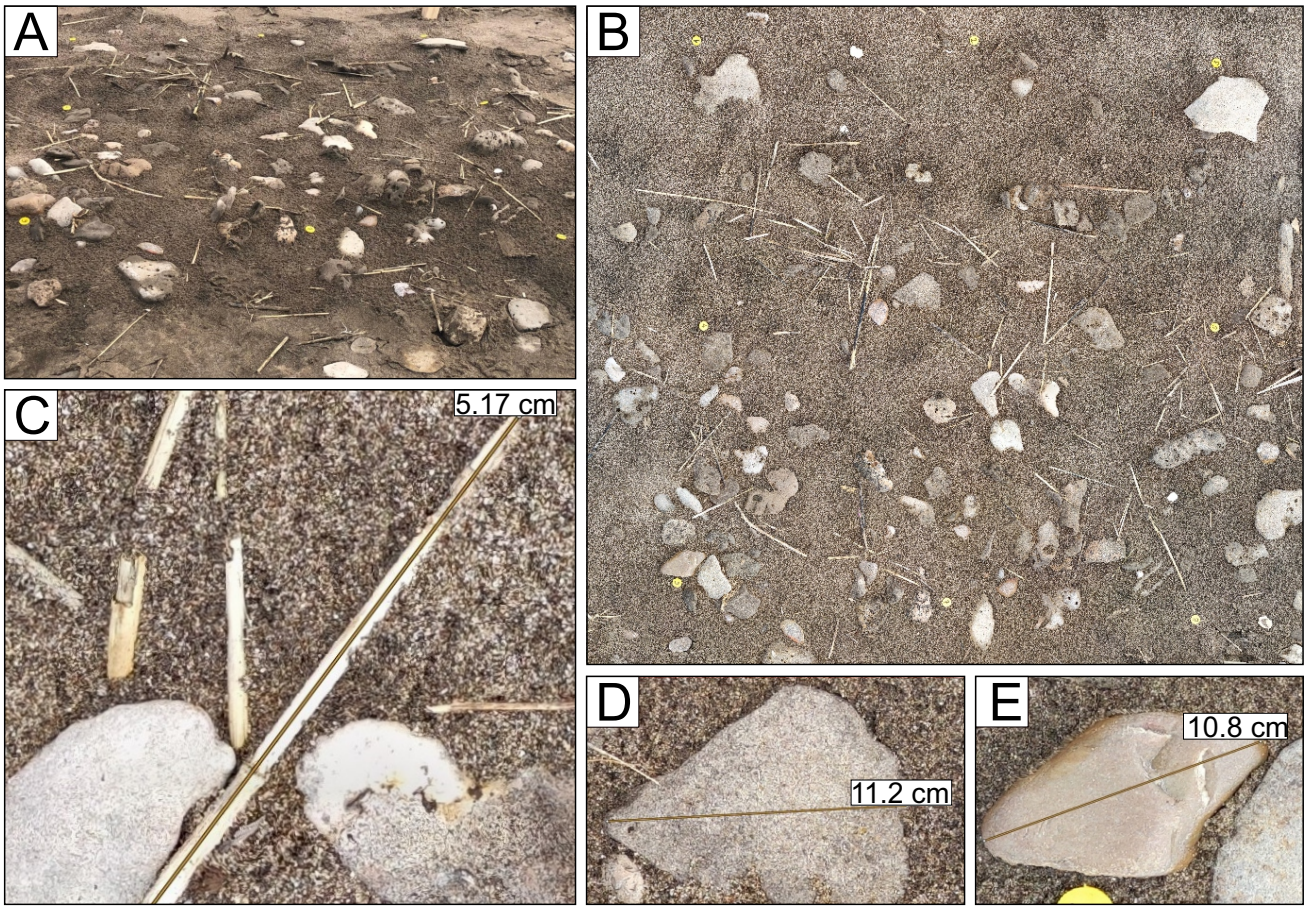

Figure 11. Results from Test sector 2. **a)** A photograph of a sandy surface with dispersed clasts on the backshore. **b)** Preliminary orthomosaic extracted using the SfM-MVS technique. Measurements of **c)**, **d)** and **e)** pebble clasts were taken on the dense point cloud. Yellow circles are the GCP and CP markers.

Finally, Sector 3 (Fig. 13a) is a complex surface showing outcrops of varying sizes ranging from 0.21 to 0.64 m (Fig. 13 c, d). Surface roughness around rocks is characterized by erosion marks and cavities of varying lengths, oriented parallel and perpendicular to the largest outcrop (Fig. 13b). The analysis on the DEM (Fig. 14a), reveals significant height variations. Maximum heights range from 0.12 to 0.16 m, with minimum elevations of 0.04 to 0.08 m, predominantly in low-lying areas and cavities. The deepest point, less than 0.04 m, is adjacent to outcrops. Height variations are displayed in microprofiles (Fig. 14b-e), where the profile corresponds to the rocky outcrop and small grooves on its sides (Fig. 14b). This differential erosion contributes significantly to the observed height discrepancies across the surface.

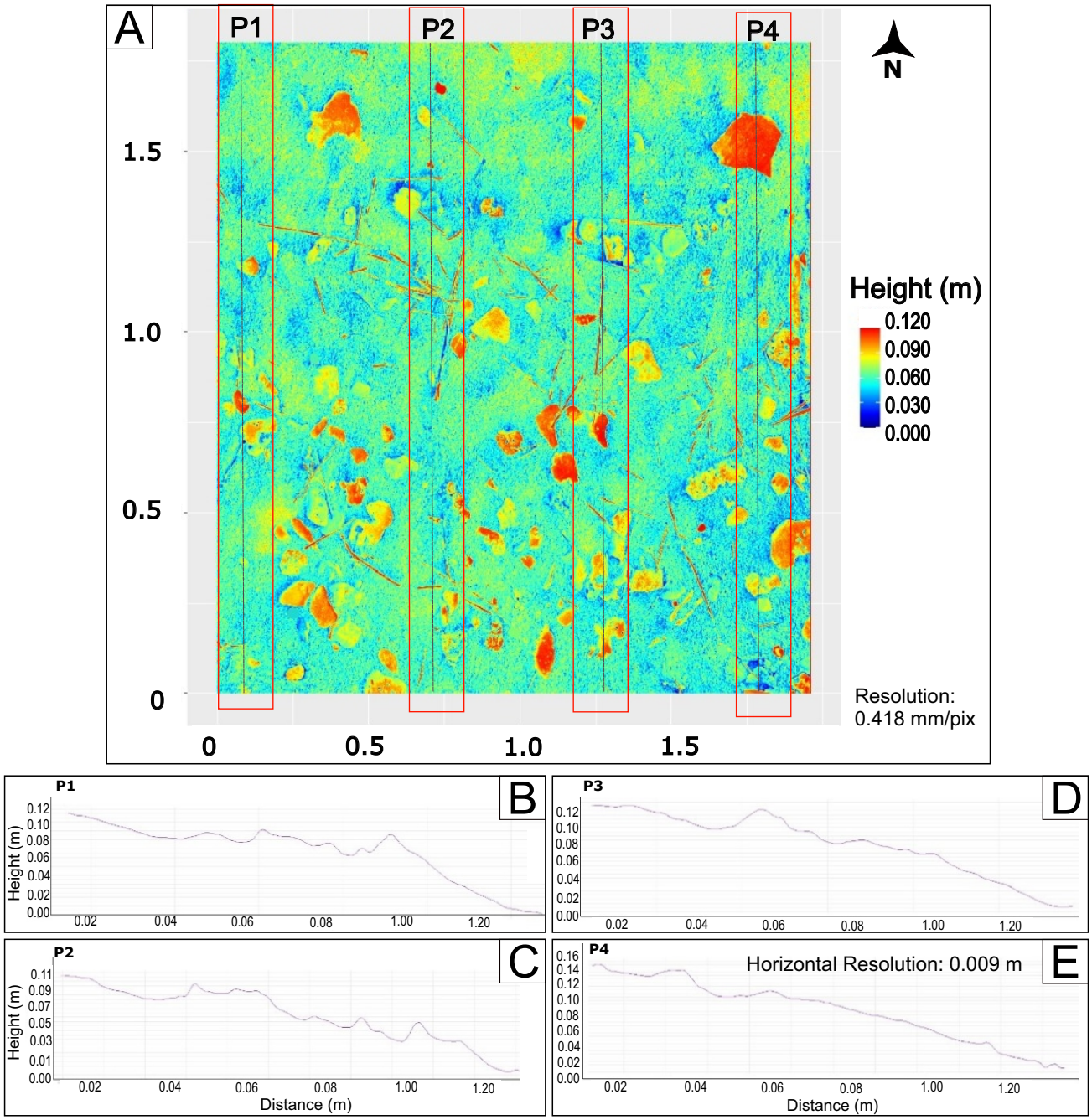

Figure 12. Results from a survey using MiSMoS at Test Sector 2. **a)** Digital Elevation Model with the position of the microprofiles P1, P2, P3 and P4 are indicated. **b)**, **c)**, **d)**, and **e)** Sections determined on a heterogeneous surface, featuring loose sand, fragments of clasts and branches.

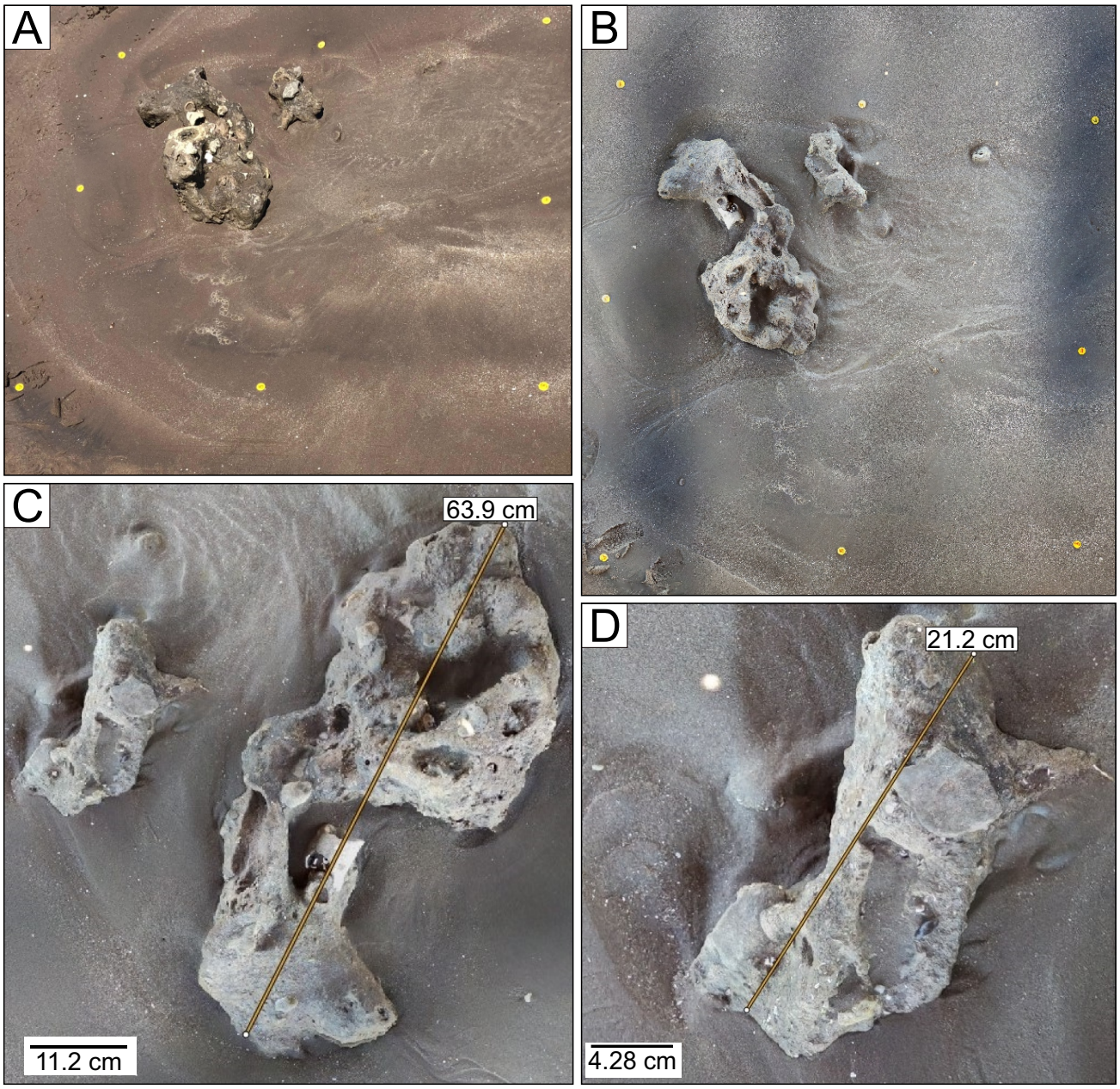

Figure 13. Results from Test sector 3. **a)** A photograph of a complex surface with differential erosion in the swash zone. **b)** Preliminary orthomosaic extracted using the SfM-MVS technique. Measurements of **c)** and **d)** were taken on the dense cloud. Yellow circles represent the CGP and CP markers.

For each test sector, the points per surface area were derived from the dense point cloud data. Test Sector 1, representing a flat surface, exhibited a point density of 5.59 points/mm^2. Test Sector 2 had a density of 5.72 points/mm^2, while Test Sector 3 reached 6.21 points/mm^2. As point density increases, the complexity of the studied surface also increases. Of the eight markers used on each surface, five were used as GCP, while three served as CP. Root Mean Square Error values indicate the discrepancy between measured and the calculated X, Y, Z coordinates (Nouwakpo *et al.*, 2019). Micromorphology precision can be determined from the height values of the CP. The minimum Root Mean Square Error value is 0.28 mm, observed at Test Sector 1; while the highest value of 10 mm is determined in Test Sector 3.

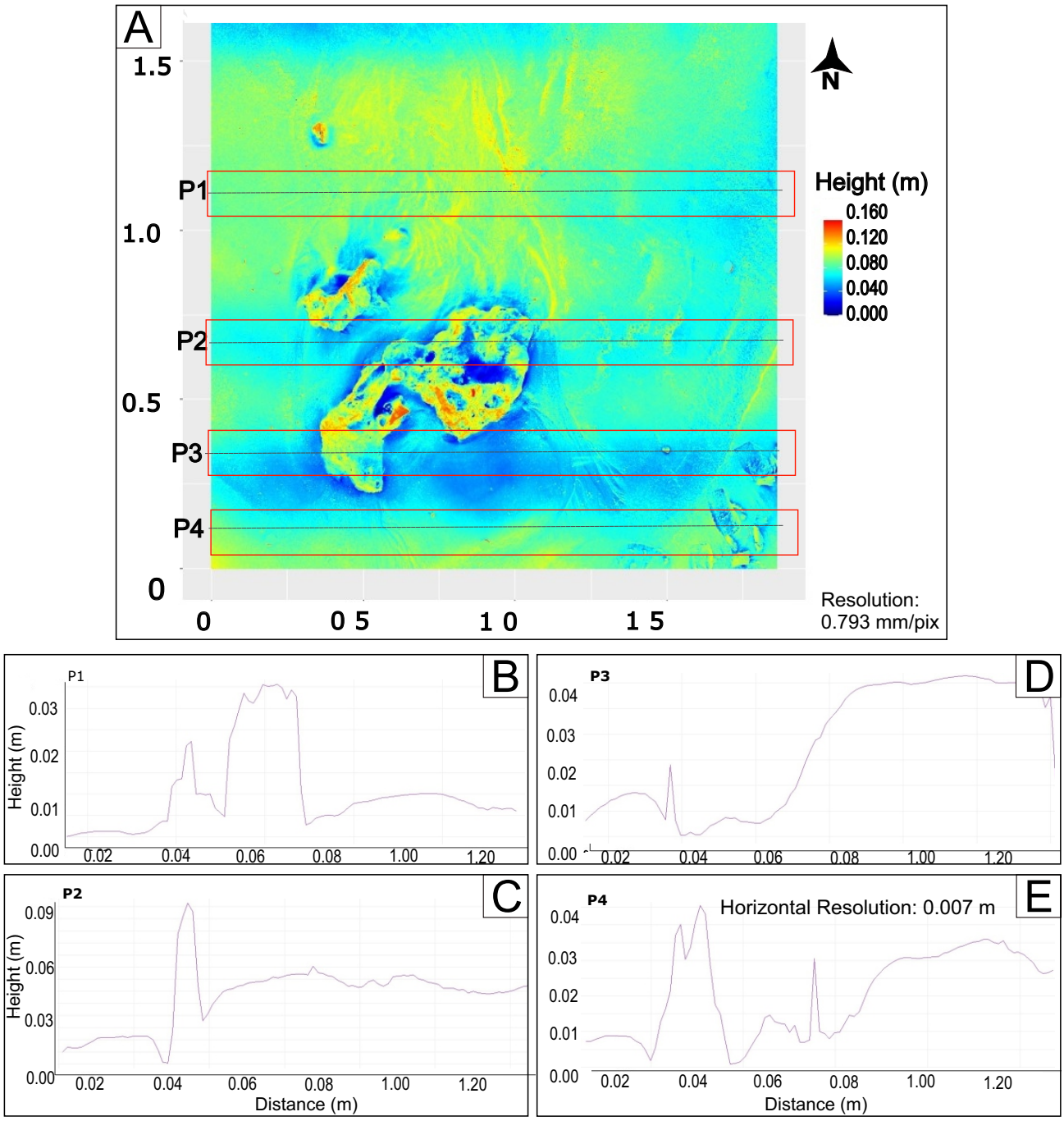

Figure 14. Results from a survey using MiSMoS at Test Sector 2. **a)** Digital Elevation Model with the position of the microprofiles P1, P2, P3 and P4 are indicated. Microprofiles of the test sector: **b)** sloping towards the beach, **c)**, **d)**, and **e)** sections determined over rocky outcrops. Combining datasets

The DEM height values were used to assess the fit of the data measured with GPS and LDM. The elevations of the CP determined in the DEM for each sector are compared with the values measured with the LDM (Fig. 15), with these data represented as scatter points. The model is fitted with linear regression to obtain the coefficient of determination of the squared error. The R^2 ranging from 0,988 to 0.993. The highest R^2 value is 0.993, close to 1.00, corresponding to Test Sector 3 (Fig. 15c).

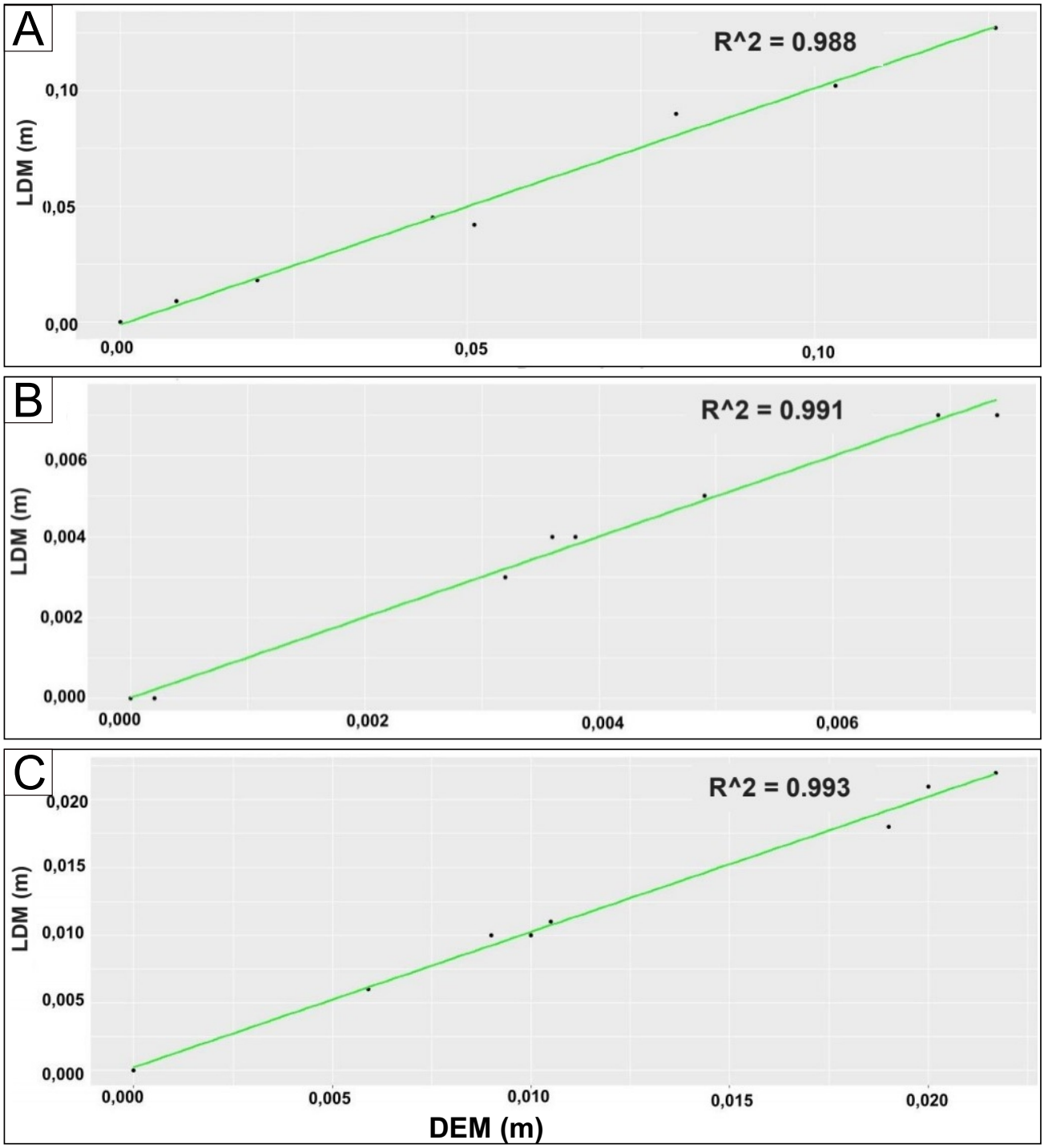

Figure 15. Trend line and coefficient of determination of the squared error obtained from heights measured with LDM at checkpoints and the values derived from the model for **a)** Test Sector 1, **b)** Test Sector 2 and **c)** Test Sector 3.

The comparison of deformation and nondeformation was represented by a red draw over the markers in the orthomosaic. The dense point cloud obtained from a set of photos taken with digital photogrammetry presented deformations in DEM (Fig. 16a). The DEM obtained with MiSMoS did not display deformations (Fig. 16b).

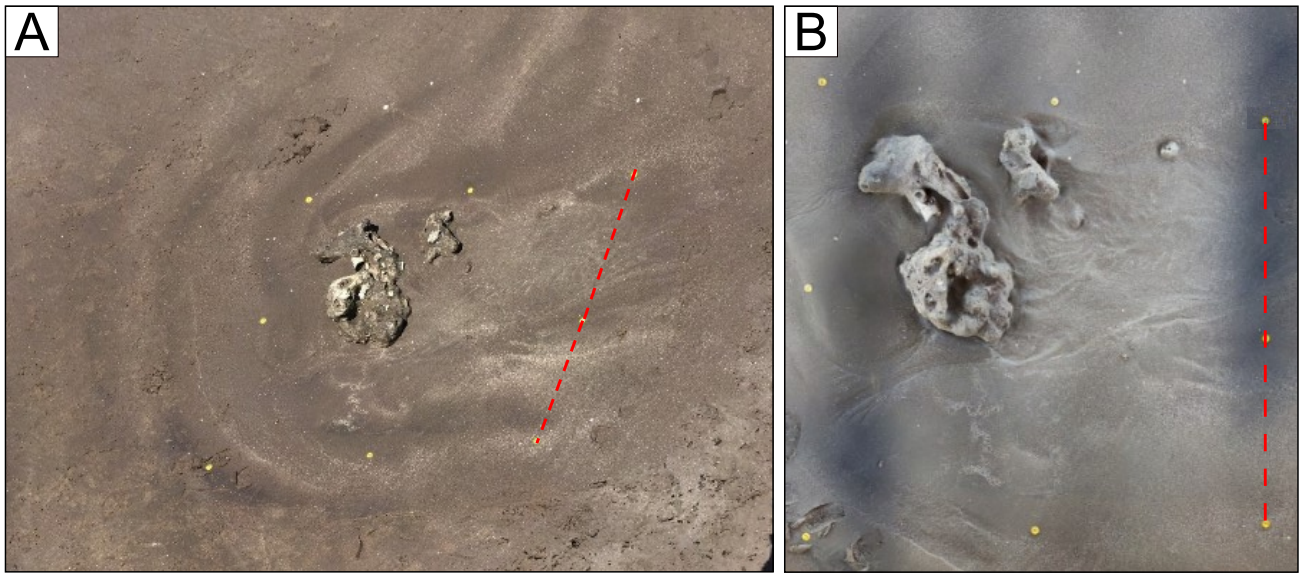

Figure 16. Orthomosaics obtained using **a)** digital photogrammetry without MiSMoS, and **b)** using MiSMoS. Red dashes indicate zones of deformation.

DISCUSSION AND CONCLUSIONS

MiSMoS, in conjunction with SfM-MVS methodology, demonstrated the ability to provide precise micromorphology data. We built a sensor-carrying structure, incorporating the two-camera system (mobile phones) and LDM. This methodology attempts to be aligned closely to make the best use of the recent developments in high resolution topographic survey (Passalacqua *et al.*, 2015).

Local surface microtopography can adjust rapidly in response to changing processes over a relatively short timescale (Foulds and Warburton, 2007). Micromorphology features in any environment represent the result of the small-scale processes that are continuously shaping the larger scale landscape. The MiSMoS micromorphology mapping was conducted in the backshore and swash zones providing detailed resolution, enabling precise identification of micromorphology features such as cavities, pebble clasts, and rock fragments (Figs. 9, 11 and 13) while avoiding the distortion of the resulting DEM.

Small variations in elevation matter when it comes to representing microtopography (Li *et al.*, 2022; Shukla *et al.*, 2023). Based on the results, once calibration is performed, MiSMoS methodology enables determination of surface variations on the order of millimeters, distributed over an area of 2.25 m^2. The microprofiles evidence this topographic variability (Figs. 10, 12 and 14). The models exhibited minimal altimetric variation, indicating the system capability to accurately capture microtopographic characteristics.

The Root Mean Square Error values indicate the discrepancy between measured and calculated coordinates (Nouwakpo *et al.*, 2014; Agüero-Vega *et al.*, 2020). The Z-coordinate values are below the millimeter range for GPC and CP, corresponding to nearly flat surfaces with minimal morphology. The coefficient of determination (R^2) was used to explain how well the DEM represents height variations. High R^2 values for all three test sectors indicate that the models effectively explain and predict height variations on surfaces with varied morphology and complexity.

The reconstruction from photos taken without any structure and at different angles did not have problems in aligning photographs, as photos captured with MiSMoS. Shadows were found during photo control on the surveyed surface. Improper lighting is attributed to the use of different angles during image capture, without a fixed angle and a structure for controlling unwanted shadows. The results indicate that imaging angle has a profound impact on accuracy and precision for data acquisition with a single camera angle in topographically complex scenes (Lane *et al.*, 1994; Nesbit and Hugenholtz, 2019).

The effects of dismissing photos with shadows, improper or varying and volatile lighting conditions within the study area results into non-uniform point clouds (Gómez-Gutiérrez *et al.*, 2014). This is associated with processing image sets with dominantly parallel viewing directions (James and Robson, 2014). The methodology developed in this work allows for a defined quadrant, whereas applying digital photogrammetry did not delimit the surface quadrant (Fig. 16b).

In this study a beach environment was selected. However, this methodology can be applied in any terrain surface with micromorphological features. Its non-intrusive nature further enhances its suitability for a wide range of applications in diverse geographical settings. The MiSMoS achieves horizontal resolutions ranging from 0.03 to 0.09 m and vertical resolutions ranging from 0.01 to 0.16 m. The simplicity, low cost and easy deployment of the MiSMoS make it a valuable tool.

Furthermore, the system is capable of recording videos for further analysis of dynamic processes such as very thin flows (less than 0.05 m). This study involves a "snapshot" micromorphological measurement, at a fixed point in time. A future study consisting of repetitive measurements on a given site will require further adjustments in order to minimize errors. As well, to select test sectors with digital photogrammetry to establish comparison with MiSMoS.

Acknowledgements. Partial support for this study was provided by funds from the MinCyT Initiative Pampa Azul project B5, MinCyT Desafio D141, and Universidad Nacional del Sur PGI 24/ZH29 The authors would like to thank reviewers and editor for valuable comments and critical review.

REFERENCES

Agüera Vega, F., Agüera Puntas, M., Martínez Carricondo, P., Mancini, F. and Carvajal, F. (20209. Effects of point cloud density, interpolation method, and grid size on derived Digital Terrain Model accuracy at micro topography level. *International Journal of Remote Sensing, 41*(21), 8281–8299. DOI: 10.1080/01431161.2020.1771788

Andes, T. (2018). *Caracterización físico-química de la descarga de agua subterránea en la playa de Pehuén Co: influencia ambiental y geomorfológica* [Unpublished Licentiate Thesis]. Universidad Nacional del Sur, 32 pp.

BOSCH, (2017). Instrucciones de Servicio. https://www.bosch-professional.com/es/es/archive/dle-50-9947-p/

Bupo, M. and Weber, J. F. (2017). Methodology for measuring micro topographies in laboratory channels with a motion sensor. *Ribagua, 4*(2), 99–109. https://doi.org/10.1080/23863781.2017.1381454

Bustos, M.L., Zilio, M., Ferrelli, F., Piccolo, M.C., Mavo Manstretta, G.M. and Perillo, G.M.E. (2021). Tourism in the COVID-19 context in mesotidal beaches: Carrying capacity for the 2020/2021 summer season in Pehuén Co, Argentina. *Ocean and Coastal Management 206*, 105584. DOI 10.1016/j.ocecoaman.2021.105584

Dagnino, J. (2014). Regresión lineal. *Revista chilena de anestesia, 43(*2), 150–153. https://doi.org/10.25237/revchilanestv43n02.15

Ehrhardt, A., Deumlich, D. and Gerke, H.H. (2022). Soil surface micro-topography by structure-from-motion photogrammetry for monitoring density and erosion dynamics. F*rontiers in Environmental Science, 9*, 737702. doi: 10.3389/fenvs.2021.737702

Foulds, S.A. and Warburton, J. (2007). Wind erosion of blanket peat during a short period of surface desiccation (North Pennines, Northern England). E*arth Surface Processes and Landforms, 32*, 481–488. https://doi.org/10.1002/esp.1422

Genchi, S., Vitale, A., Perillo, G. and Delrieux, C. (2015). Structure-from-Motion Approach for Characterization of Bioerosion Patterns Using UAV Imagery. *Sensors, 15(*2), 3593–3609. doi:10.3390/s150203593

Gómez-Gutiérrez, A., Schnabel, S., Berenguer Sempere, F., Lavado Contador, F., Rubio and Delgado, J. (2014). Using 3D photo-reconstruction methods to estimate gully headcut erosion. *Catena 120*, 91–101. doi:10.1016/j.catena.2014.04.004.

Hasmanda, M., and Riha, K. (2012). The modelling of stereoscopic 3D scene acquisition. *Radioengineering, 21*(1), 134–142. ISSN 1805-9600

James, M.R., and Robson, S. (2014). Mitigating systematic error in topographic models derived from UAV and ground-based image networks. Earth Surf. Process. *Landforms, 39*, 1413–1420. https://doi.org/10.1002/esp.3609

Lane, S.N., Richards, K.S., and Chandler, J.H. (1994). Developments in monitoring and modelling small□scale river bed topography. *Earth Surface Processes and Landforms, 19*(4), 349–368. https://doi.org/10.1002/esp.3290190406

Li, Y., Lu, X., Washington Allen, R. A., and Li, Y. (2022). Microtopographic controls on erosion and deposition of a rilled hillslope in eastern Tennessee, USA. *Remote Sensing, 14*(6), 1315. https://doi.org/10.3390/rs14061315

Matias, B., Oliveira, H., Almeida, J., Dias, A., Ferreira, H., Martins, A., and Silva, E. (2015). High-accuracy low-cost RTK-GPS for an unmanned surface vehicle. Oceans, Genova, *Italy*, 1–4, doi: 10.1109/OCEANS-Genova.2015.7271673.

Miles, J., Thorpe, A., Russell, P., and Masselink, G. (2014). Observations of bedforms on a dissipative macrotidal beach. *Ocean Dynamics 64*, 225–239. https://doi.org/10.1007/s10236-013-0677-2

Nakata, Y., Iwasaki, K., Shimoda, S., and Torita, H. (2023). Understanding microtopography changes in agricultural landscapes through precision assessments of digital surface models by the UAV-RTK-PPK method without ground control points. *Smart Agricultural Technology*, 100–269. https://doi.org/10.1016/j.atech.2023.100269

Nesbit, P.R., and Hugenholtz, C.H. (2019). Enhancing UAV-SfM 3D Model Accuracy in High-Relief Landscapes by Incorporating Oblique Images. *Remote Sensing, 11*(3), 1–24. doi:10.3390/rs11030239

Nouwakpo, S. K., James, M. R., Weltz, M. A., Huang, C. H., Chagas, I., and Lima, L. (2014). Evaluation of structure from motion for soil microtopography measurement. *The photogrammetric record, 29*(147), 297–316. DOI:10.1111/phor.12072

Nouwakpo, S. K., Weltz, M.A., and McGwire, K. (2016). Assessing the performance of structure-from-motion photogrammetry and terrestrial LiDAR for reconstructing soil surface microtopography of naturally vegetated plots. *Earth Surfaces Processes and Landforms 41*, 308–322. DOI: 10.1002/esp.3787

Nouwakpo, S.K., Toledo, D., Sanderson, M., and Weltz, M. (2019). Understanding the effects of grazing and prescribed fire on hydrology of Kentucky bluegrass–dominated rangelands in the northern Great Plains. *Journal of Soil and Water Conservation, 74*, 360-371. 10.2489/jswc.74.4.360.

Otvos, E.G. (1999). Rain-induced beach processes; landforms of ground water sapping and surface runoff. *Journal of Coastal Research, 15*(4), 1040–1054. https://www.jstor.org/stable/4299023

Passalacqua, P., Belmont, P., Staley, D. M., Simley, J. D., Arrowsmith, J. R., Bode, C. A., Crosby, C, DeLong, S. B., Glenn, N. F., Kelly S. A., and Lague, D. (2015). Analyzing high resolution topography for advancing the understanding of mass and energy transfer through landscapes: A review. *Earth-Science Reviews, 148*, 174−193. https://doi.org/10.1016/j.earscirev.2015.05.012

Perillo, G.M.E., and Piccolo, M.C (2011). Global Variability in Estuaries and Coastal Settings. In: E. Wolanski and D.S. McLusky (eds.), *Treatise on Estuarine and Coastal Science*, Vol 1, pp. 7–36. Waltham: Academic Press. 10.1016/B978-0-12-374711-2.00102-9.

Perillo, G.M.E., Nuciari, L., Alquinga Salazar, Y.C., Genchi, S.A., Perillo, V.L., and Piccolo, M.C. (2022). MiSMoS: a microscale morphology system. In *Proceedings of the II Particles in the Americas Conference*: 24.

Remondino, F., and Fraser, C. (2006). Digital Camera Calibration Methods: Considerations and Comparisons. International Archives of Photogrammetry. *Remote Sensing and Spatial Information Sciences, 36*(5), 266–27. https://doi.org/10.3929/ethz-b-000158067

Sherman, D. J., Short, A. D., and Takeda, I. (1993). Sediment mixing-depth and bedform migration in rip channels. *Journal of coastal research 15*, 39–48. ISSN 0749-0208. DOI: 10.2307/25735722

Shukla, T., Tang, W., Trettin, C. C., Chen, G., Chen, S., and Allan, C. (2023). Quantification of microtopography in natural ecosystems using close-range remote sensing. *Remote Sensing, 15*(9), 2387. DOI:10.3390/rs15092387

Turner, I. L., Russell, P. E., and; Butt, T. (2008). Measurement of wave-by-wave bed-levels in the swash zone. *Coastal Engineering, 55*(12), 1237–1242. doi:10.1016/j.coastaleng.2008.09.009